

Article

Dynamic Feature Identification of Carbon-Fiber-Reinforced Polymer Laminates Based on Fiber Bragg Grating Sensing Technology

Cong Chen ¹ , Hua-Ping Wang ^{1,2,*} , Jie Ma ¹ and Maihemuti Wusiman ¹

¹ School of Civil Engineering and Mechanics, Lanzhou University, Lanzhou 730000, China; chenc21@lzu.edu.cn (C.C.); majie15927274099@163.com (J.M.); 220220936411@lzu.edu.cn (M.W.)

² Key Laboratory of Special Functional Materials and Structural Design, Ministry of Education, Key Lab of Mechanics on Disaster and Environment in Western China, Ministry of Education, Lanzhou University, Lanzhou 730000, China

* Correspondence: wanghuaping1128@sina.cn or hpwang@lzu.edu.cn

Abstract: Carbon-fiber-reinforced polymer (CFRP) composites have many advantages, and have been widely used in aerospace structures, buildings, bridges, etc. The analysis of dynamic response characteristics of CFRP composite structures is of great significance for promoting the development of smart composite structures. For this reason, vibration experiments of CFRP laminates with surface-attached fiber Bragg grating (FBG) sensors under various dynamic loading conditions were carried out. Time- and frequency-domain analyses were conducted on the FBG testing signals to check the dynamic characteristics of the CFRP structure and the sensing performance of the installed sensors. The results show that the FBG sensors attached to the surface of the CFRP laminates can accurately measure the dynamic response and determine the excited position of the CFRP laminates, as well as invert the strain distribution of the CFRP laminates through the FBG sensors at different positions. By performing Fourier transform, short-time Fourier transform, and frequency domain decomposition (FDD) on the FBG sensing signals, the time–frequency information and the first eight modal frequencies of the excited CFRP structure can be obtained. The modal frequencies obtained by different excitation types are similar, which can be used for structural damage identification. The research in this paper clarifies the effectiveness and accuracy of FBG sensors in sensing the dynamic characteristics of CFRP structures, which can be used for performance evaluation of CFRP structures and will effectively promote the design and development of intelligent composite material structures.

Keywords: CFRP laminates; FBG sensor; dynamic response; time and frequency analysis; frequency domain decomposition method



Citation: Chen, C.; Wang, H.-P.; Ma, J.; Wusiman, M. Dynamic Feature Identification of Carbon-Fiber-Reinforced Polymer Laminates Based on Fiber Bragg Grating Sensing Technology. *Buildings* **2023**, *13*, 2292. <https://doi.org/10.3390/buildings13092292>

Academic Editor: Harry Far

Received: 21 July 2023

Revised: 22 August 2023

Accepted: 6 September 2023

Published: 8 September 2023



Copyright: © 2023 by the authors. Licensee MDPI, Basel, Switzerland. This article is an open access article distributed under the terms and conditions of the Creative Commons Attribution (CC BY) license (<https://creativecommons.org/licenses/by/4.0/>).

1. Introduction

CFRP composites have been widely used in aerospace structures, high-speed railway systems (i.e., roofs and train bodies), building structures, wind turbines, gas turbine vehicles, and ocean engineering due to their high strength, light weight, corrosion resistance, and flexible design [1–3]. For practical engineering projects, infrastructures are constantly in the process of aging due to combined action of increased loads, environmental influences, and design and quality control deficiencies. If these aging structures are not inspected and maintained in time, the local damage in the structures will be gradually propagated, leading to huge disasters for the structures and their surrounding environments.

To prevent the deterioration process of these aging structures and extend their service life, strengthening and repairing technologies are more environmentally and economically preferable to direct replacement of the damaged structures. One of the widely accepted approaches is to use externally bonded CFRP composites on the tensile surfaces of the beam structures to improve the flexural, shear, and load-bearing capabilities of reinforced

structures [4,5]. This is a competitive alternative to traditional reinforcement methods. However, it requires that the real-time and long-term performance of CFRP components should be reasonably designed and controlled. Therefore, there is a high demand for structural health monitoring (SHM) of CFRP-assembled structures to track structural state, damage, and degradation.

Regarding the monitoring of lightweight and high-strength materials such as CFRP, non-contact methods, including digital image correlation, 3D laser vibrometers, etc., are widely used techniques. Francesconi et al. [6] used speckle interferometry and digital image correlation techniques to study the comprehensive internal displacement field and eigenmodes of different geometric structures, and compared the outcomes with the finite element simulation results. Guinchard et al. [7] performed modal analysis of lightweight structures using an advanced laser scanning vibrometer system. However, these methods rely on environmental conditions and structural surface properties, and the equipment is complex, making it difficult to achieve real-time monitoring in actual operating structures.

As one of the advanced optical fiber sensors, the FBG sensor has the characteristics of light weight, small size, absolute measurement, integrated signal sensing and transmission, and anti-electromagnetic interference [8–11]. FBG sensing technology can provide unique technical advantages for the health monitoring of CFRP composites.

Considerable attempts have been conducted using FBG sensors to monitor CFRP structures. Panopoulou et al. [12] identified the damage to a composite antenna through FBG data, based on experimental modal analysis and neural network technology. Tserpes et al. [13,14] established a relationship between the strain measured by FBG sensors and the health of composite structures through finite element analysis and experimentation. Lu et al. [15,16] extracted damage characteristics of a CFRP structure through Fourier transform and principal component analysis, and studied the low-speed collision location algorithm based on FBG sensors using the arrival time difference of the precursor wave and support vector machine. Rezayat et al. [17] proposed the variable selection least square method to locate and reconstruct impact force based on measured vibration data. Zhao et al. [18] proposed the sum of the square of the K-order deviation to predict the low-speed impact position through the dynamic strain signal obtained by FBG sensors. Geng et al. [19] used Fourier transform and neural network technology to extract parameters from FBG signals for identifying CFRP structural damage. Datta et al. [20] predicted the location of impact events and estimated energy based on a least square support vector regression algorithm. Falcatelli et al. [21] studied the application of strain modal test based on an FBG sensor in an automobile composite structure. In general, the current research mainly focuses on developing suitable algorithms to extract load and damage identification parameters from FBG signals for assessing the health state of composite structures. Some scholars have also carried out the assembly of CFRP composite materials and optical fiber sensing elements to configure smart CFRP components [22]. It is worth noting that due to the complexity of actual engineering, these algorithms have limitations in tracking random attack or damage. Analysis on the dynamic response characteristics of composite structures based on FBG sensing signals still requires further exploration [23,24]. Therefore, it is of great significance to study the dynamic response characteristics of composite structures under different working conditions through FBG sensors to promote the development of smart composite structures assembled with self-sensing, identification, and rehabilitation functions.

In view of the above analysis, this paper studies the dynamic response characteristics of CFRP laminates with FBGs attached to the upper and bottom surfaces under the excitation of sinusoidal frequency sweep, rectangular pulse sweep, periodic rectangular pulse, and sinusoidal fixed frequency vibration. Time- and frequency-domain analysis were performed on the testing data to evaluate the structural performance of the structures and the sensing performance of the FBG sensors. Meanwhile, suggestions for the design of an FBG sensing network and smart CFRP structures are given through the analysis of the monitoring data.

2. Experimental Model

To explore the dynamic response of CFRP composites, CFRP laminates assembled with surface-attached FBG sensors were fabricated. The testing sample was made of T700 12K carbon braiding fabric prepreg with an area of $450 \times 450 \text{ mm}^2$, a thickness of 3 mm, and a weight of 832 g. The stacking sequence of each CFRP sheet was $[0/90/0/90/0/90]$. Based on the comprehensive consideration of practical application scenarios and experimental convenience, the constraint of the CFRP laminates was conducted with the four corners fixed by a clamp, which can be regarded as the fixed support constraints. The experimental setup of the dynamic tests is shown in Figure 1. FBG sensors were symmetrically pasted on the two surfaces of the CFRP laminates by flexible adhesive and numbered FBG1–FBG19, as shown in Figure 1c,d. The location coordinates and laying angles of each FBG sensor are shown in Table 1. The laying angle was 0° in the horizontal direction, and the counterclockwise direction was the positive direction. These sensors were connected to an optical fiber interrogator (si255) to form a test system. The sampling frequency of the optical fiber interrogator was 5 kHz.

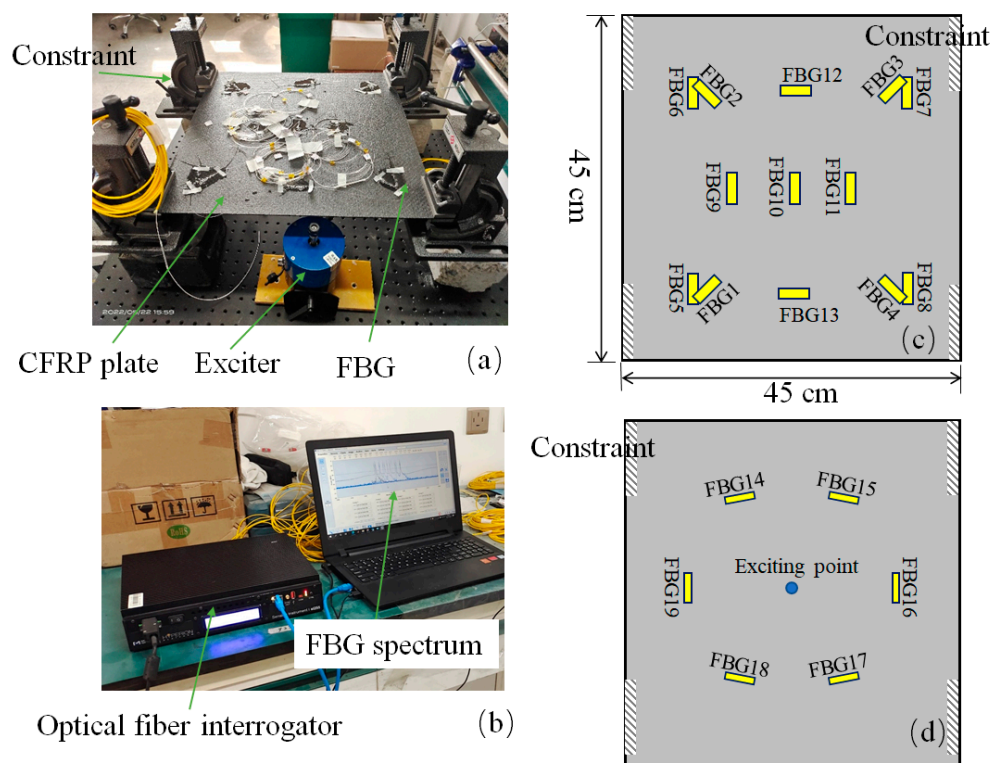


Figure 1. Experimental setup: (a) Physical photo of the testing system; (b) optical fiber interrogator; (c) FBG layout on the upper surface of the CFRP laminate; (d) FBG layout on the bottom surface of the CFRP laminate.

To check the dynamic response of the CFRP laminates under various loading conditions, four different dynamic loads (i.e., sinusoidal frequency sweep, rectangular pulse frequency sweep, periodic rectangular pulse, and 100 Hz sinusoidal fixed frequency vibration) were applied to the center point of the CFRP laminates through the exciter. The loading method of sine sweep and rectangular pulse sweep was that the loading frequency increased linearly from 1 to 2500 Hz within 3 min. The loading frequency of periodic rectangular pulses was 1 Hz, and the duration of the single rectangular pulse was 0.3 s. The loading time of the 100 Hz sinusoidal constant frequency vibration lasted for about 6 min. Since the experiment was carried out indoors with a relatively short loading time, the temperature field of the testing environment was considered as constant. Therefore, the

temperature effect on the sensing signals of the FBG sensors can be ignored [25,26], and no additional temperature compensation measure was required during the testing.

Table 1. Position coordinates of the installed FBG sensors.

Item	<i>x</i> (cm)	<i>y</i> (cm)	Laying Angle	Distance to Excitation Point (cm)
FBG1	7.5	7.5	45°	21.2
FBG2	7.5	37.5	−45°	21.2
FBG3	37.5	37.5	45°	21.2
FBG4	37.5	7.5	−45°	21.2
FBG5	6	7.5	90°	22.3
FBG6	6	37.5	90°	22.3
FBG7	39	37.5	90°	22.3
FBG8	39	7.5	90°	22.3
FBG9	14.25	22.5	90°	8.25
FBG10	22.5	22.5	90°	0
FBG11	30.75	22.5	90°	8.25
FBG12	22.5	39	0°	16.5
FBG13	22.5	6	0°	16.5
FBG14	15.5	34.6	30°	13.98
FBG15	29.5	34.6	−30°	13.98
FBG16	36.5	22.5	90°	14
FBG17	29.5	10.4	30°	13.98
FBG18	15.5	10.4	−30°	13.98
FBG19	8.5	22.5	90°	14

3. Time-Domain Analysis

Since the FBG sensors were symmetrically installed on the laminates, the testing data provided by a partial analysis of the FBG sensors can be considered to check the dynamic performance of the CFRP composites. Therefore, the measured signals of FBG1, FBG5, FBG10-FBG12, and FBG19 were selected for the data analysis.

3.1. Sine Frequency Sweep Condition

The process of linear sine sweep excitation can be expressed as [27]:

$$s(t) = \sin[\theta(t)] = \sin\left(\omega_1 t + \frac{\omega_2 - \omega_1}{T} \cdot \frac{t^2}{2}\right) \quad (1)$$

where $s(t)$ is a linear sine sweep and $\theta(t)$ is the argument of the sine function. ω_1 and ω_2 are the start and end frequencies, respectively, and T is the duration in seconds. The instantaneous frequency $\omega(t)$ is given by

$$\omega(t) = \frac{d[\theta(t)]}{dt} = \omega_1 + \frac{\omega_2 - \omega_1}{T} \cdot t \quad (2)$$

The start frequency of this excitation is 1 Hz, the end frequency is 2500 Hz, and the duration is 180 s. Figure 2 shows a schematic diagram of the excitation from 0 to 1.8 s.

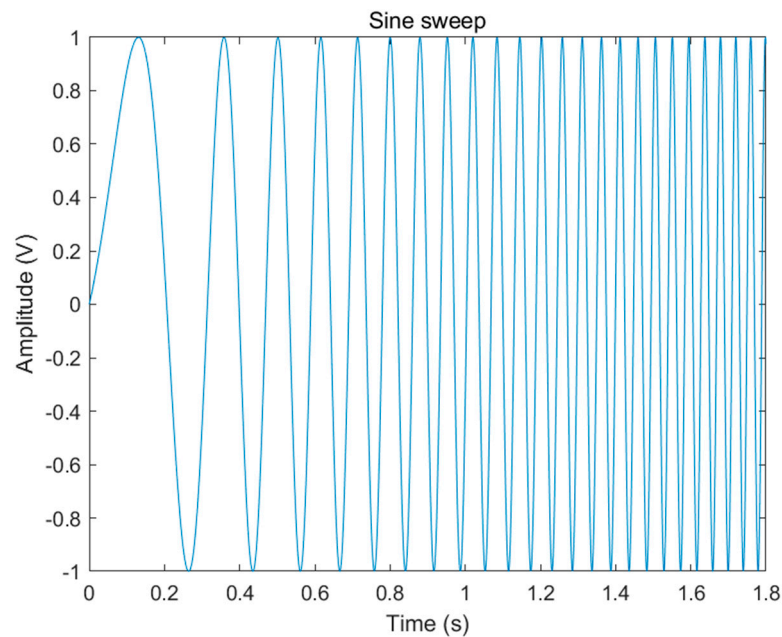


Figure 2. Sine sweep excitation.

Figure 3 shows the wavelength increment of each FBG sensor in the time domain under the condition of sinusoidal frequency sweep. It can be seen that the FBG signals at different positions have similar trends. The wavelength increment of the FBG under the sinusoidal frequency sweep load is reciprocating, and large oscillations exit at individual time points, which indicates that the FBG sensors can sensitively monitor the sinusoidal frequency sweep load. The large oscillations generated by each sensor at individual time points are due to the fact that the frequency of the loading just reaches the natural frequency of the CFRP laminates, and a resonance phenomenon occurs. It can be seen from Figure 3a,c–e that the sensors closer to the excitation point suffer from greater signal amplitude, which indicates that the location of the excitation point can be judged by comparing the signal amplitudes of FBG sensors at different positions. Comparing Figure 3a,b, it can be seen that although FBG1 and FBG5 were located in the same position, they had different signal amplitudes due to the different axial angles. This indicates that the sensitivity of the FBG sensors to various directions is different, and the direction with the greatest sensitivity is along the axial direction of the FBG sensing element. Figure 3f shows the signal of the FBG sensor pasted on the bottom surface of the laminates under the condition of sinusoidal frequency sweep. The same phenomenon as that of the FBG sensor pasted on the upper surface is observed, which shows that the pasted surface does not affect the monitoring effect of the FBG.

3.2. Rectangular Pulse Frequency Sweep Condition

The frequency range and duration of the rectangular pulse frequency sweep excitation are the same as the sinusoidal frequency sweep excitation, which is linearly swept from 1 Hz to 2500 Hz within 3 min. The waveform of the excitation is different. Figure 4 shows the schematic diagram of the rectangular pulse frequency sweep excitation. Different from the gentle change of the sinusoidal frequency sweep excitation, the rectangular pulse sweep frequency excitation has the characteristic of mutation.

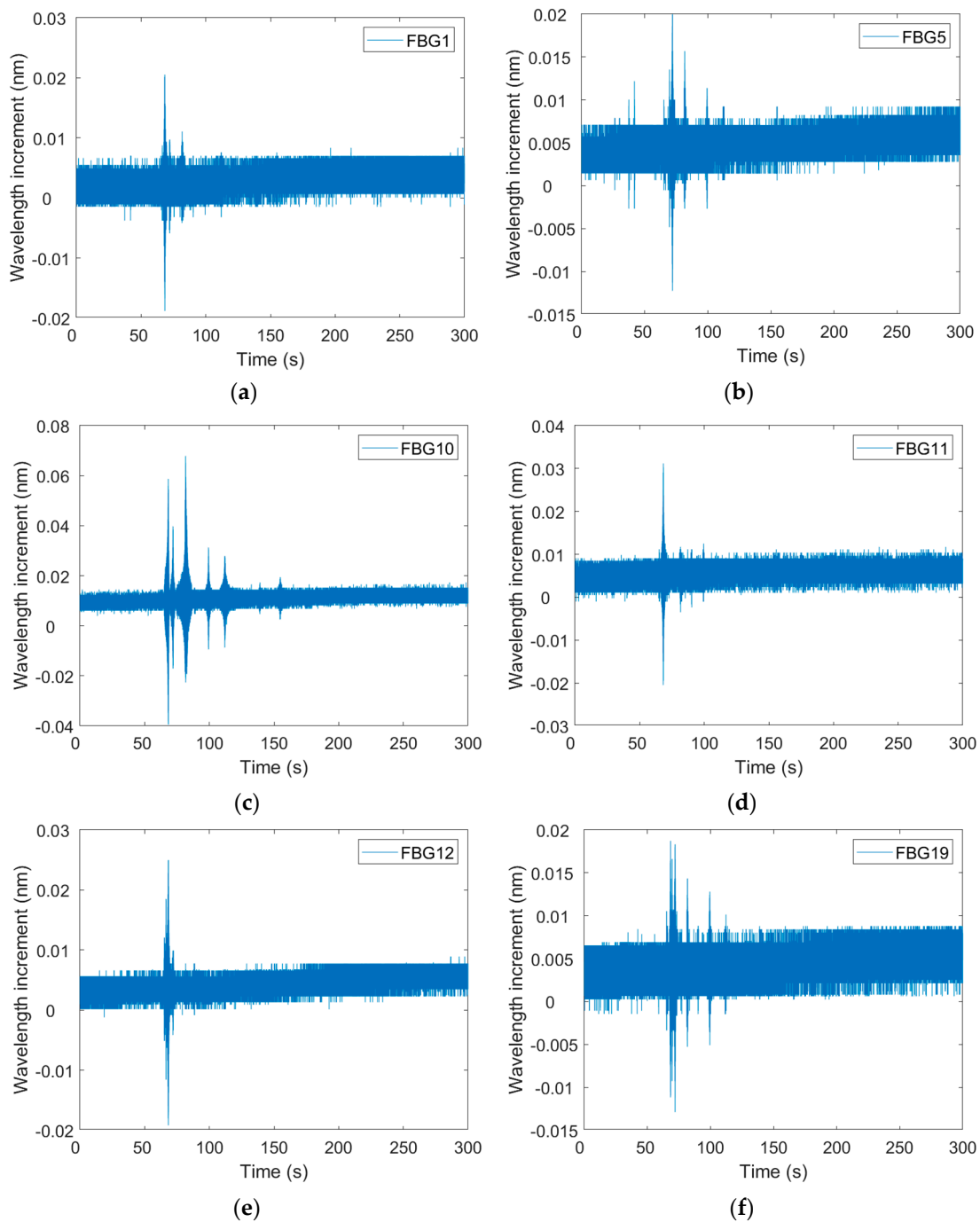


Figure 3. Signals of FBG sensors under sine sweep condition: (a) FBG1; (b) FBG5; (c) FBG10; (d) FBG11; (e) FBG12; (f) FBG19.

Figure 5 shows the wavelength increment time-domain diagram of each sensor under the condition of pulse frequency sweep. The FBG signals at different positions have similar waveforms, which are similar to those of the sinusoidal frequency sweep condition. The wavelength increment of FBG under sinusoidal loading is reciprocating, and there are large oscillations at individual time points, which shows that the FBG sensor can sensitively monitor the application of sinusoidal sweeping load. The large oscillations generated by each sensor at individual time points are due to the fact that the frequency of loading just reaches the natural frequency of the CFRP laminates, and a resonance phenomenon occurs. Due to the small loading magnitude of the pulse sweep, only the signals of FBG10 pasted at the loading point have the largest amplitude, and the signal amplitude differences

of the other FBGs are not obvious. Figure 5f shows the signal of the FBG pasted on the bottom surface of the laminates under the condition of sinusoidal frequency sweep. It can be seen that the variation phenomenon is similar to that of the FBG sensor pasted on the upper surface, which shows that the pasted surface does not affect the monitoring effect of the FBG.

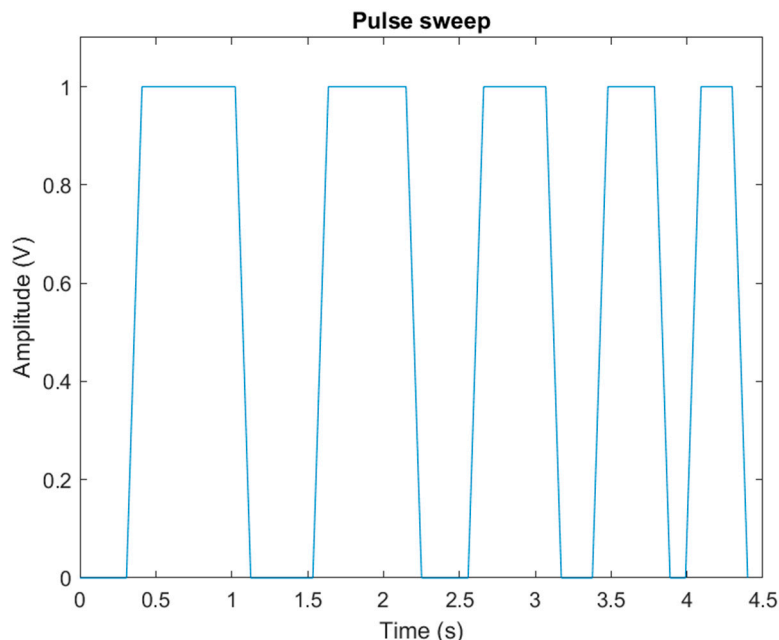


Figure 4. Pulse sweep excitation.

3.3. Periodic Rectangular Pulse Condition

The process of periodic rectangular pulse excitation $f(t)$ can be expressed as [28]:

$$f(t) = \begin{cases} 1 & nT - \frac{\tau}{2} < t < nT + \frac{\tau}{2} \\ 0 & nT + \frac{\tau}{2} < t < (n + 1)T - \frac{\tau}{2} \end{cases}, f > 0, n = 0, 1, 2, \dots \quad (3)$$

where T is the period, and τ is the width of the rectangle. In this test, the values of the two parameters are 1 s and 0.3 s, respectively. Figure 6 shows a schematic diagram of the periodic rectangular pulse excitation. A burst of 0.3 s excitation was applied every 1 s. Since the excitation time is very short, the action can be approximated to perform an impact on the CFRP laminates every 1 s.

Figure 7 shows the wavelength increment time-domain diagram of each sensor under the condition of periodic rectangular pulse. The FBG signals at different positions have similar waveforms. The wavelength increment of the FBG is vibrating back and forth under the condition of pulse sweep frequency loading. The signal vibration amplitude of the FBG increases at 150 s, which is because the loading magnitude was increased midway through the experiment. Meanwhile, comparing Figure 7a,c–e, the sensor closer to the excitation point has the greater signal amplitude, which shows that the location of the excitation point can be judged by comparing the signal amplitudes of FBG sensors at different positions. Figure 7f shows the signal of the FBG sensor pasted on the bottom surface of the board under the condition of periodic rectangular pulse. It can be seen that the variation phenomenon is the same as that of the FBG sensor pasted on the upper surface, which indicates that the thickness of the CFRP laminates has an ignorable effect on the monitoring signals of FBG sensors.

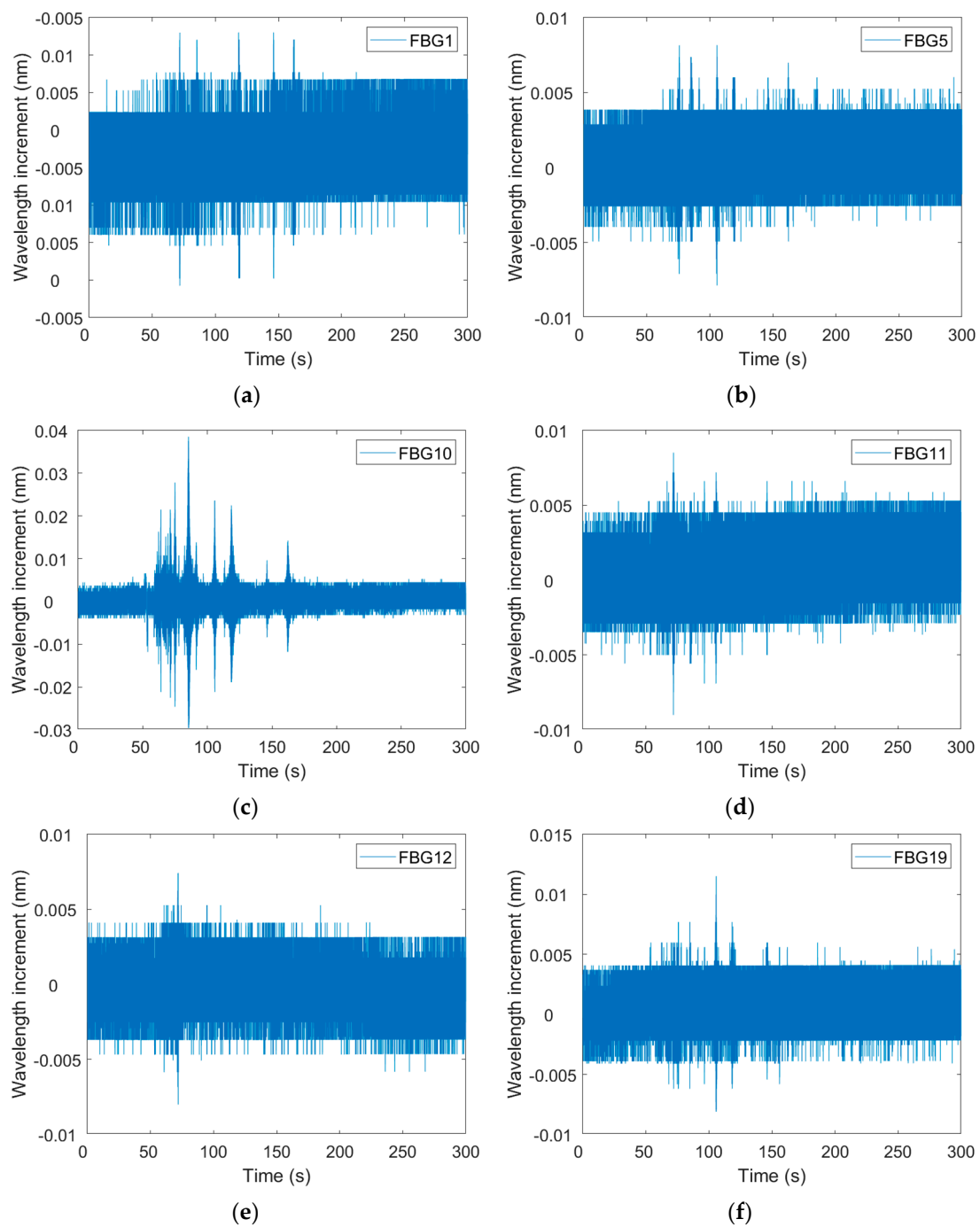


Figure 5. Signals of FBG sensors under pulse sweep condition: (a) FBG1; (b) FBG5; (c) FBG10; (d) FBG11; (e) FBG12; (f) FBG19.

The loading parameters of the periodic rectangular pulse condition are equivalent to impacting the CFRP laminates every 1 s. In order to clearly check the FBG signal of CFRP laminates under a single impact, the image of Figure 7c is enlarged to the time interval of 0.3 s, as shown in Figure 8. It can be seen that under the action of a single impact, the wavelength increment of FBG reaches the maximum at the moment of impact, then decays rapidly and oscillates stably at the initial value.

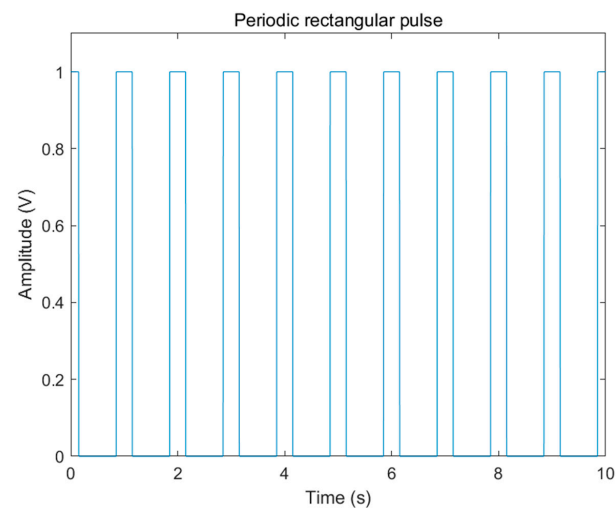


Figure 6. Periodic rectangular pulse excitation.

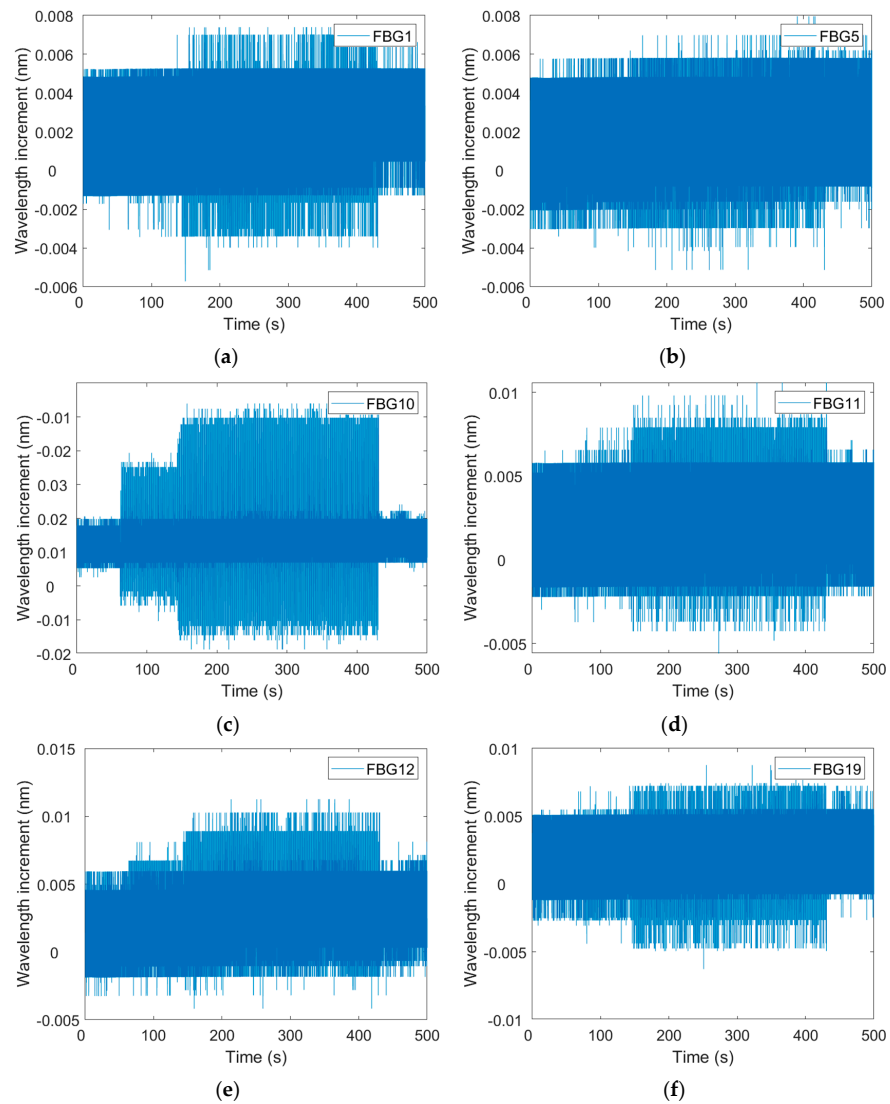


Figure 7. Signals of FBG sensors under rectangular pulse condition: (a) FBG1; (b) FBG5; (c) FBG10; (d) FBG11; (e) FBG12; (f) FBG19.

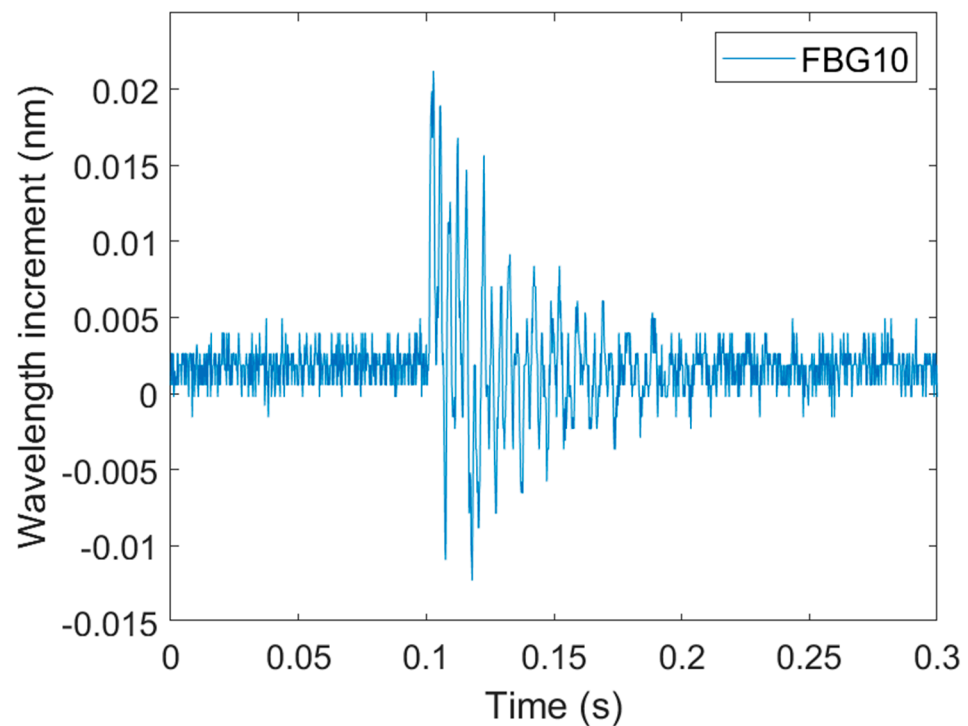


Figure 8. FBG signal distribution under single impact.

3.4. Condition of 100 Hz Sinusoidal Fixed Frequency Vibration

Figure 9 shows the wavelength increment time-domain diagram of each sensor under the condition of 100 Hz sinusoidal constant frequency vibration. The FBG signals at different positions have similar waveforms. It can be seen from Figure 9 that when the load is applied, the wavelength increments of the FBGs reciprocate stably, and the amplitudes of the reciprocating vibration are the same. When the loading is stopped, the FBG signal returns to the initial value, which proves the sensing performance of FBG sensors for long-term monitoring of CFRP laminates.

3.5. Summary of Time-Domain Analysis

To understand the spatial response characteristics of the CFRP laminates with FBG sensors attached to the surfaces under dynamic excitation, an analysis path was selected, which passed through FBG5, FBG13, FBG9, FBG10, FBG11, FBG12, and FBG7 at once (see the red line in Figure 10). Then, the responses of each sensor on the analysis path at the dangerous moment of each working condition were extracted for the comparison analysis. The wavelength increments of each sensor under each working condition were firstly marked on the graph, then connected by a spline curve to obtain the response change diagram of the CFRP laminates under each working condition, as shown in Figure 11. The abscissa in the figure is the distance from each sensor to the excitation point, and the ordinate is the wavelength increment of the sensor. The response characteristics of the CFRP laminates under various working conditions can be straightforwardly declared. The largest response is at the excitation point, and the response farther away from the excitation point is relatively smaller. However, the response of sensors near the constraint increases due to the constraint on the displacement of the CFRP laminates. This is consistent with the mechanical behavior of CFRP laminates and also proves the effectiveness of the monitoring function of FBG sensors.

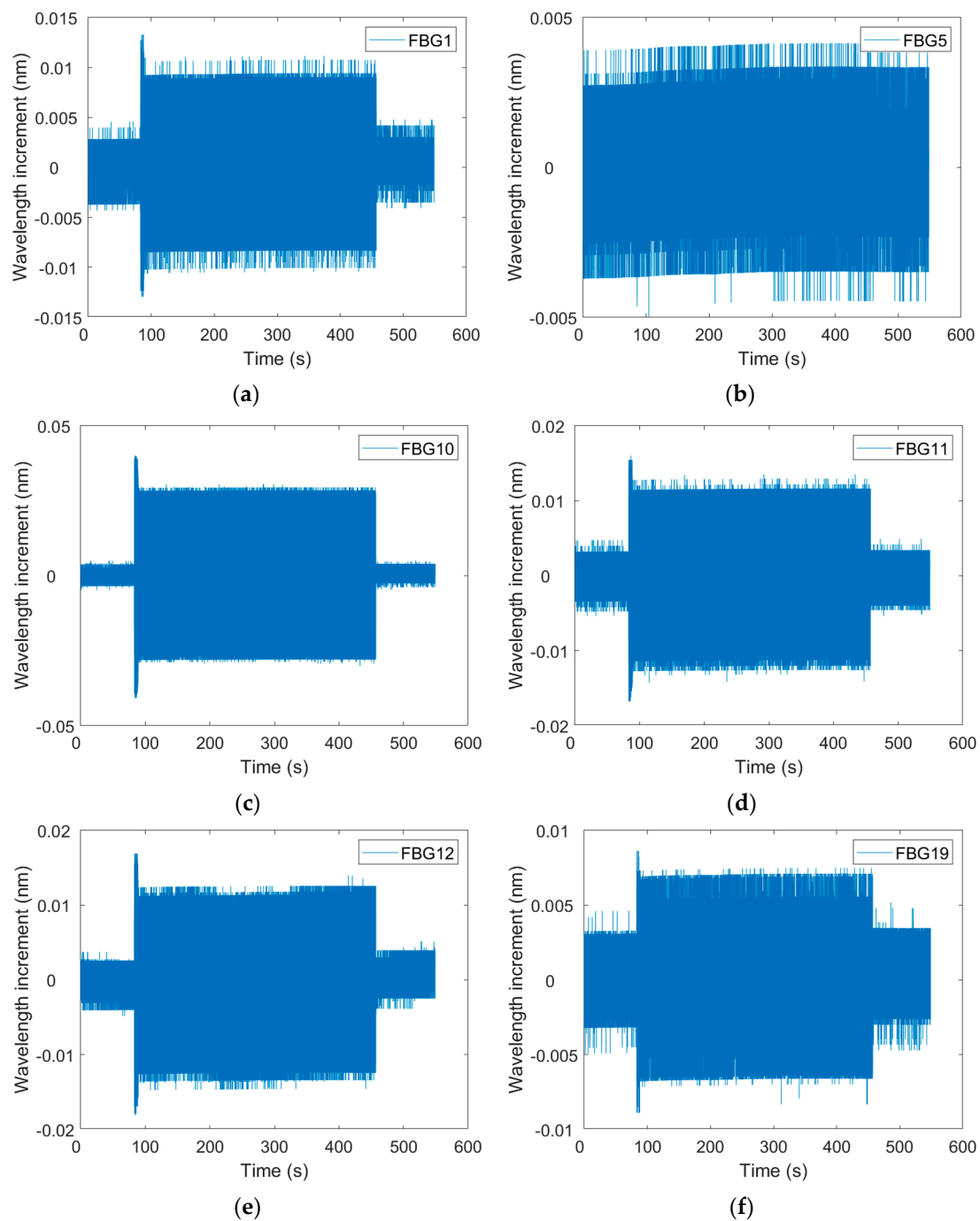


Figure 9. Signals of FBG sensors under 100 Hz sine fixed frequency vibration condition: (a) FBG1; (b) FBG5; (c) FBG10; (d) FBG11; (e) FBG12; (f) FBG19.

The spatial response characteristics of CFRP laminates were studied through path analysis, which is reasonable for analyzing beam structures. For CFRP square laminates, since the response characteristics in both the length and width directions are important for structural evaluation, it would be more effective to obtain a two-dimensional response distribution feature field. To construct the characteristic field of response distribution, a dangerous moment (i.e., the moment with the maximum wavelength increment) was selected in each working condition, and MATLAB was used to perform surface interpolation on the response value measured by the FBG sensors at that moment. Figure 12 shows the distribution characteristic field of the wavelength increment of the FBG sensors on the CFRP laminates under various working conditions.

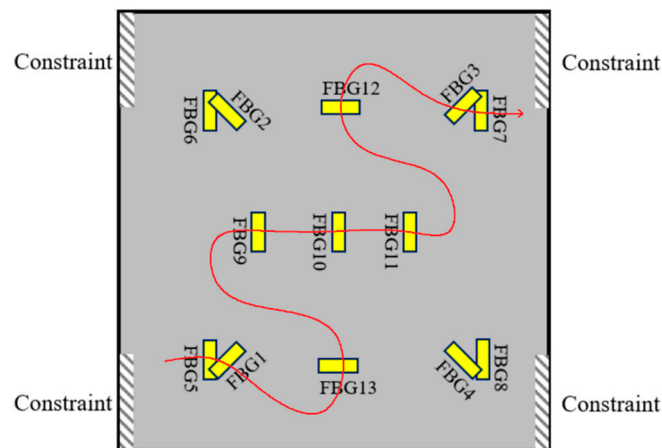


Figure 10. Analysis path.

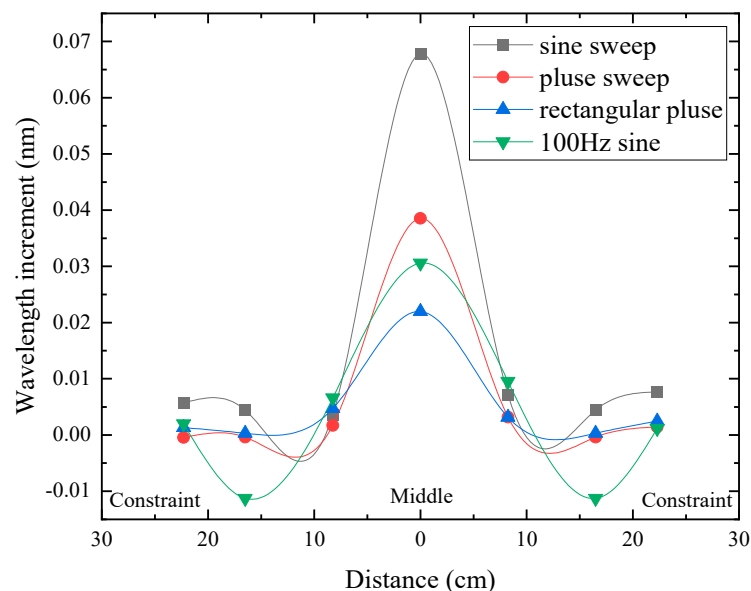


Figure 11. Response changes of FBG sensors under various working conditions.

Figure 12 shows the response distribution characteristics of the CFRP laminates under various working conditions. The maximum response is at the excitation point, and the response farther away from the excitation point is much smaller. It is also worth noting that the response at the four corners of the CFRP laminates also increased due to the constraint effect. The response characteristics of the above-mentioned CFRP laminates conform to the mechanical behavior of the CFRP laminates. This means that the constructed response characteristic field can accurately characterize the stress–strain field of the CFRP laminates under dynamic actions.

To verify the potential of the FBG sensor to reconstruct the stress–strain field of CFRP laminates, a finite element analysis (FEA) was established based on the commercial software ABAQUS 2022. Figure 13 shows the stress field under a point load in the laminates. Interestingly, the stress field generated by FEA follows the same pattern as the response characteristic field in Figure 12, which verifies the reliability of the FBG sensor to reconstruct the stress field of CFRP laminates. Due to the diversity of CFRP laminates induced by the complicated fabrication, the quantitative analysis between the simulated results and the testing results has not been conducted. The dynamic performance identification of the practical CFRP laminates can be realized by making full use of the FBG sensing technology.

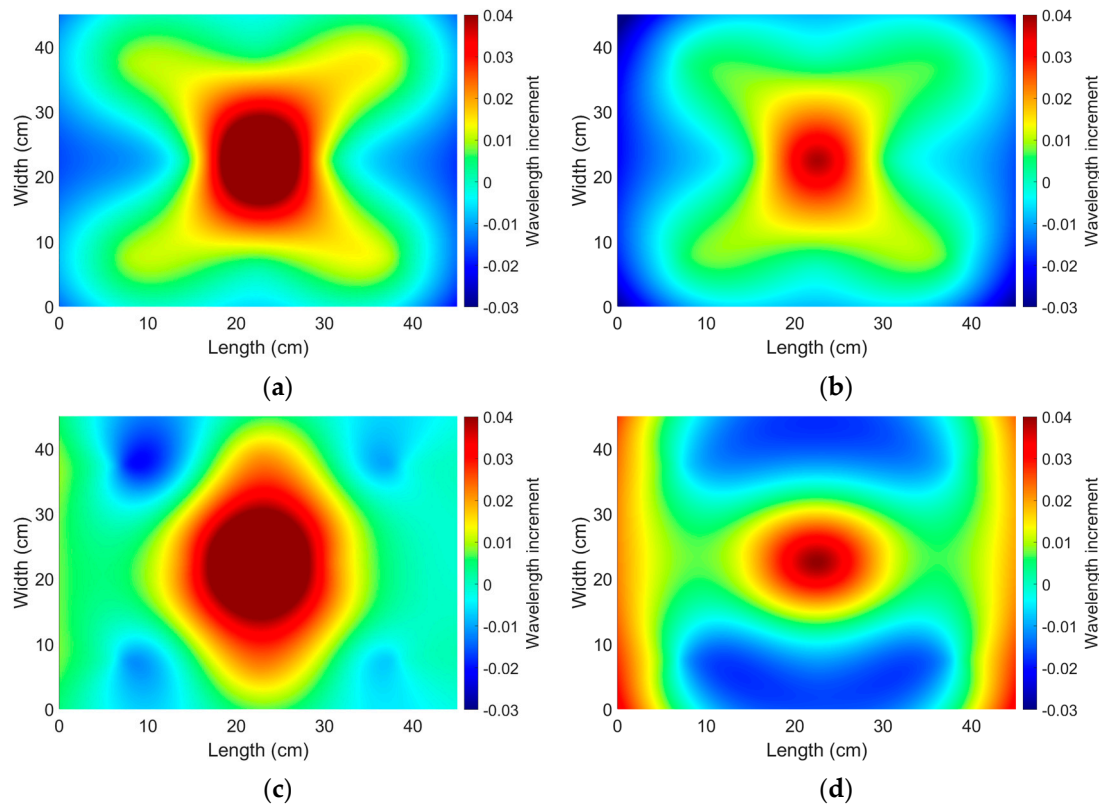


Figure 12. Wavelength increment distribution characteristics: (a) Sine sweep condition; (b) pulse sweep condition; (c) rectangular pulse condition; (d) 100 Hz sine.



Figure 13. Stress field diagram of FEA of CFRP laminates under mid-point load.

4. Frequency-Domain Analysis

Given the above analysis, it can be seen that the FBG sensor can accurately detect the dynamic response signal of CFRP laminates. However, it is difficult to identify the state and dynamic characteristics of the CFRP laminates based only on time-domain signals. Therefore, it is necessary to further analyze the frequency-domain information. Therefore, Fourier transform, short-time Fourier transform, and frequency domain decomposition have been adopted to analyze the FBG signals in the frequency domain.

4.1. Fourier Transform Analysis

One of the effective tools for frequency-domain analysis on vibration signals is to obtain the power spectral density (PSD) of the signal through Fourier transform [29]. Through the power spectrum, the probability distribution of the vibration energy of the signal in

each frequency domain can be obtained. The formula for power spectrum estimation using the periodogram method is as follows [29]:

$$X[k] = \sum_{n=0}^{N-1} x[n]e^{-k\frac{2\pi ni}{N}}, k = 0, 1, \dots, N - 1 \quad (4)$$

$$I_N(k) = I_N(\omega)|_{\omega=\frac{2\pi k}{N}} = \frac{1}{N} |X(k)|^2, k = 0, 1, \dots, N - 1 \quad (5)$$

where $X[k]$ is the frequency-domain distribution of the signal, $x[n]$ is the time-domain distribution of the signal, and $I_N(k)$ is the power spectrum estimation of the signal. Figures 14–17 show the power spectral density of FBG1 and FBG10 under four loading conditions.

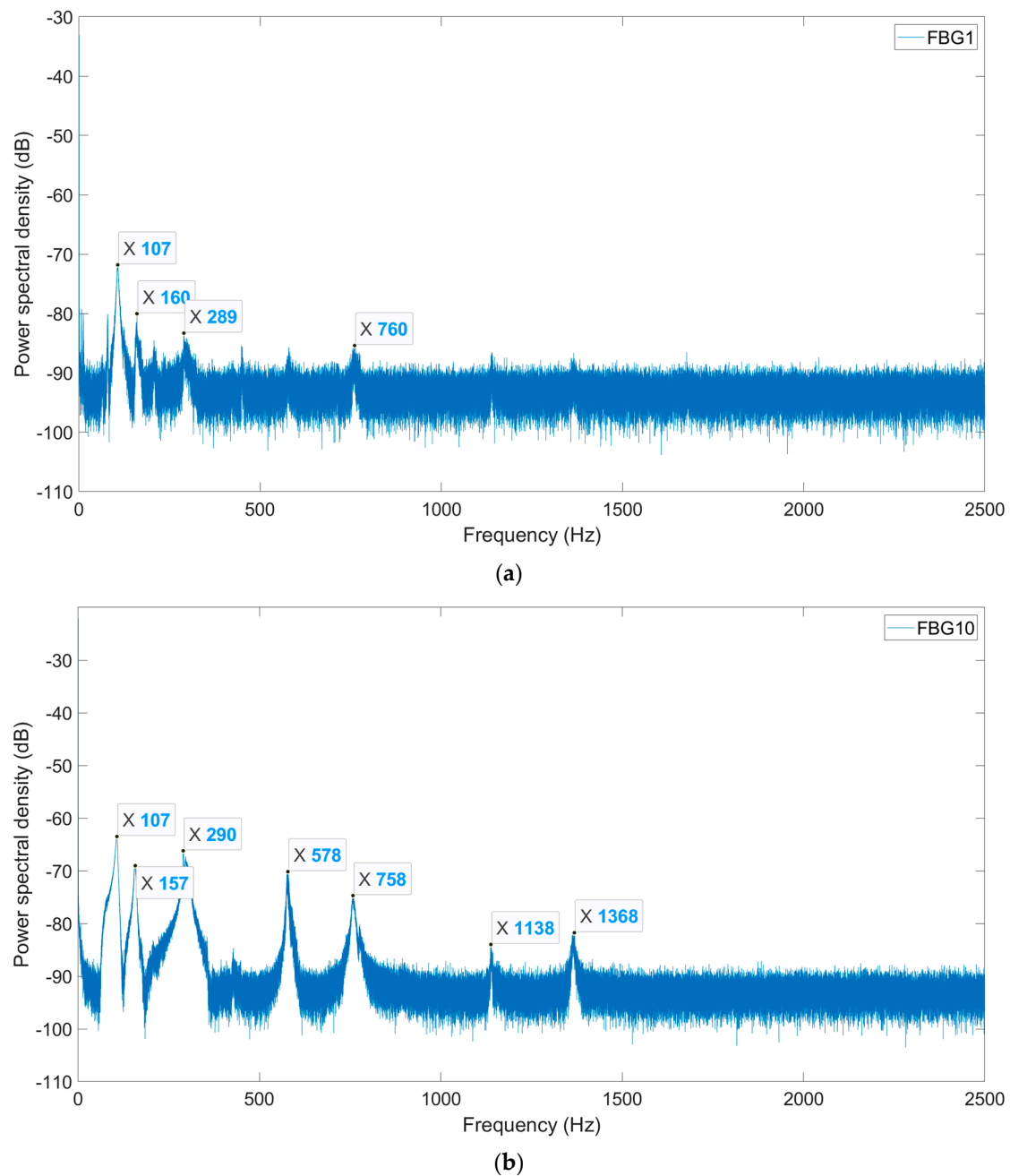


Figure 14. PSD under sine sweep condition: (a) FBG1; (b) FBG10.

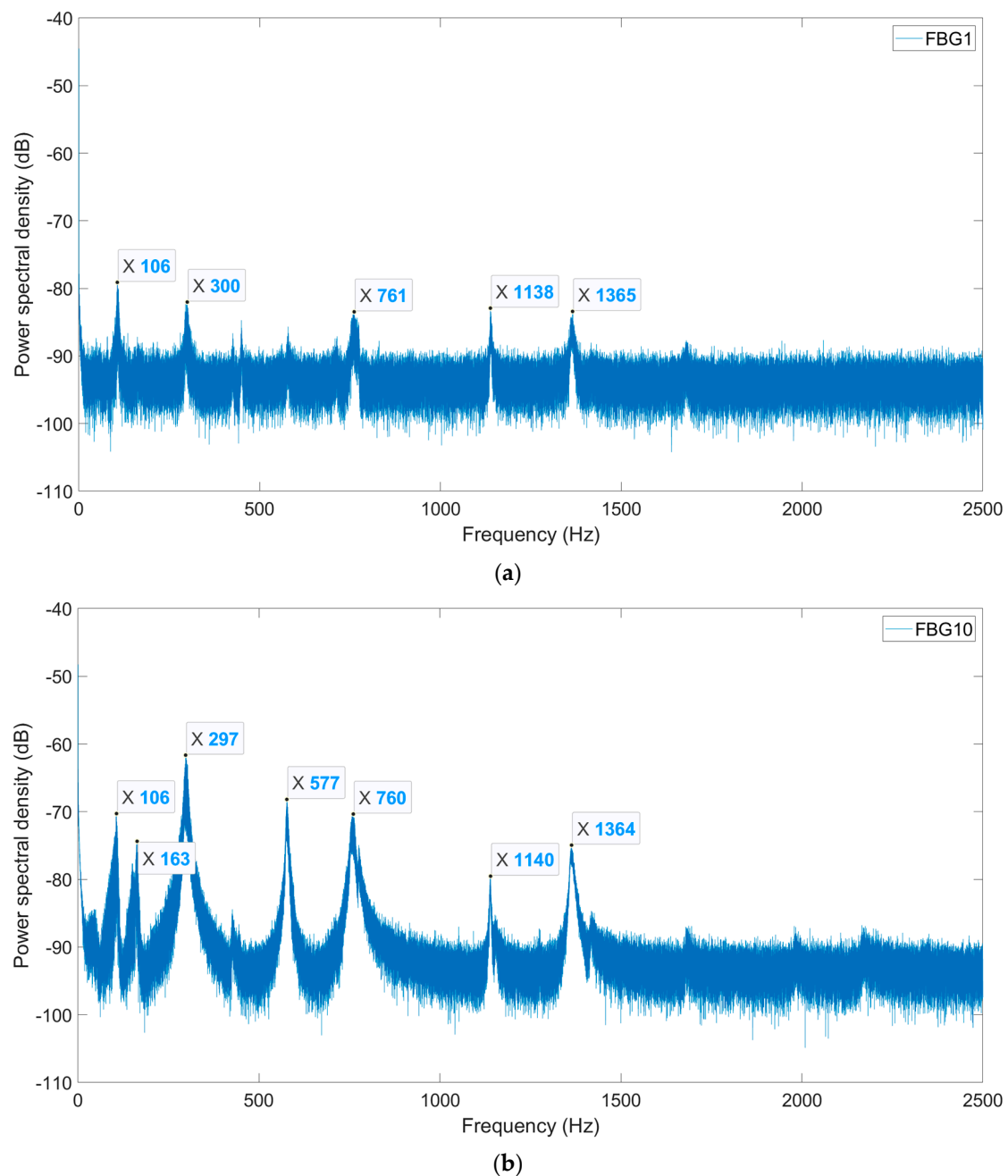


Figure 15. PSD under pulse sweep condition: (a) FBG1; (b) FBG10.

Comparing Figures 14–16, it can be seen that the signal power spectra of the same FBG under sinusoidal sweep, rectangular pulse sweep, and periodic rectangular pulse conditions are similar, and the peak frequencies and quantities in the power spectra are also similar. Among them, the peak frequencies of the power spectra of FBG10 are concentrated around 106 Hz, 160 Hz, 295 Hz, 578 Hz, 760 Hz, 1140 Hz, and 1365 Hz. This is because the peak frequency of the signal power spectrum under the frequency sweep and impact test represents the natural frequency of the structure. The peak frequency is the frequency point with the largest amplitude in the signal power spectrum, which reflects the frequency at which the structure is most likely to resonate when it vibrates freely. When the external excitation frequency is close to the natural frequency of the structure, the resonance effect will cause a sharp increase in the amplitude, which will appear as an obvious peak in the signal power spectrum. At the same time, since the CFRP laminates were not damaged during the test, the natural frequency did not change. It is also worth noting that the

signal power spectrum of the FBG is more concentrated at the peak under the sinusoidal frequency sweep condition, followed by the rectangular pulse frequency sweep condition, and the case under periodic rectangular pulse condition is the most dispersed. This is because the principle of Fourier transform is to combine sine (cosine) functions of different frequencies, so the applied excitation type closer to the sine function brings about the more concentrated Fourier transform result. In addition, under the three working conditions, the power spectrum peak value of FBG10 is more obvious than that of FBG1. This is because the signal change of FBG10 in the time domain is more obvious than that of FBG1. This also indicates that selecting sensors with significant changes in the time-domain signal for Fourier transform will obtain more effective frequency-domain information.

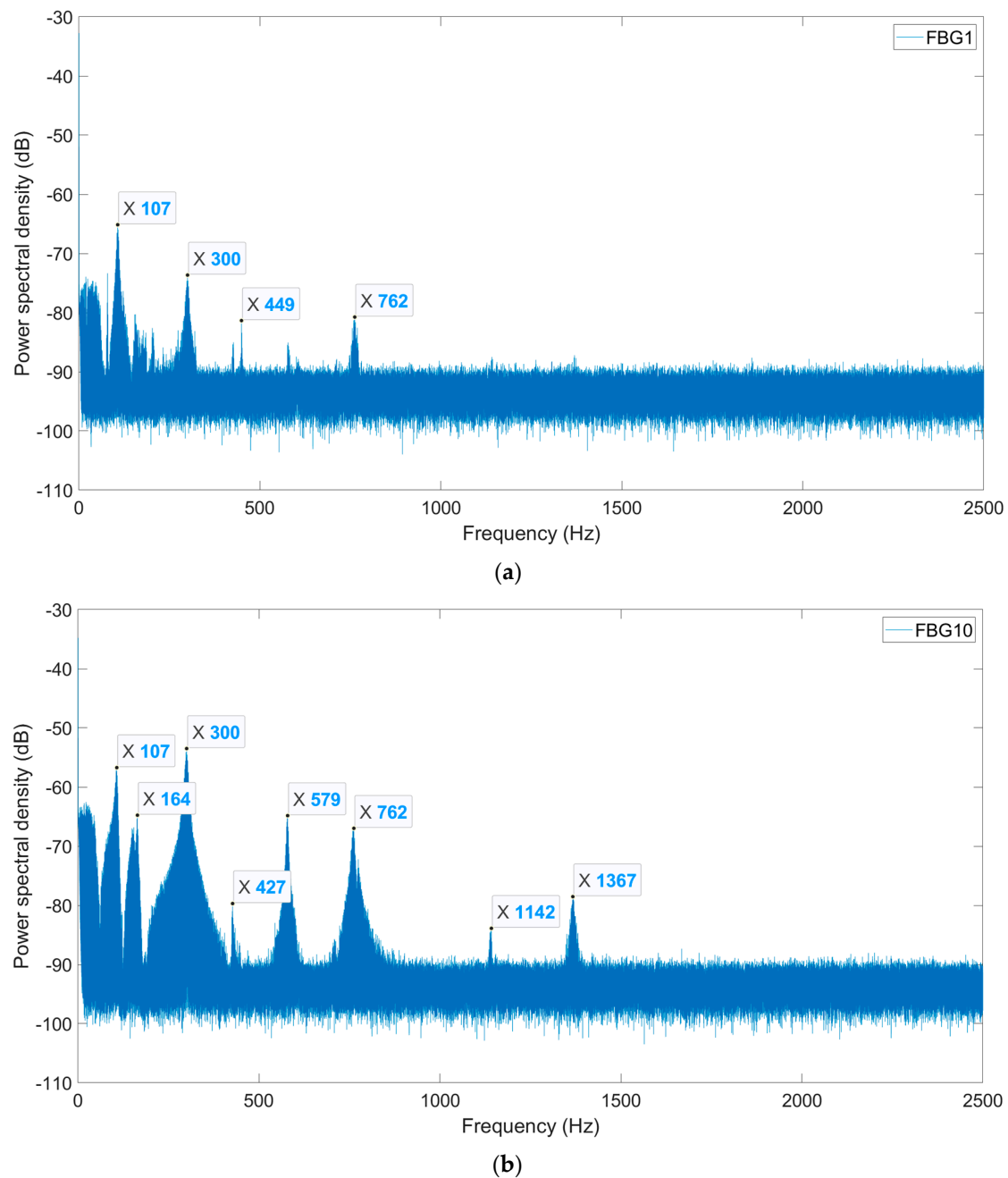


Figure 16. PSD under periodic rectangular pulse condition: (a) FBG1; (b) FBG10.

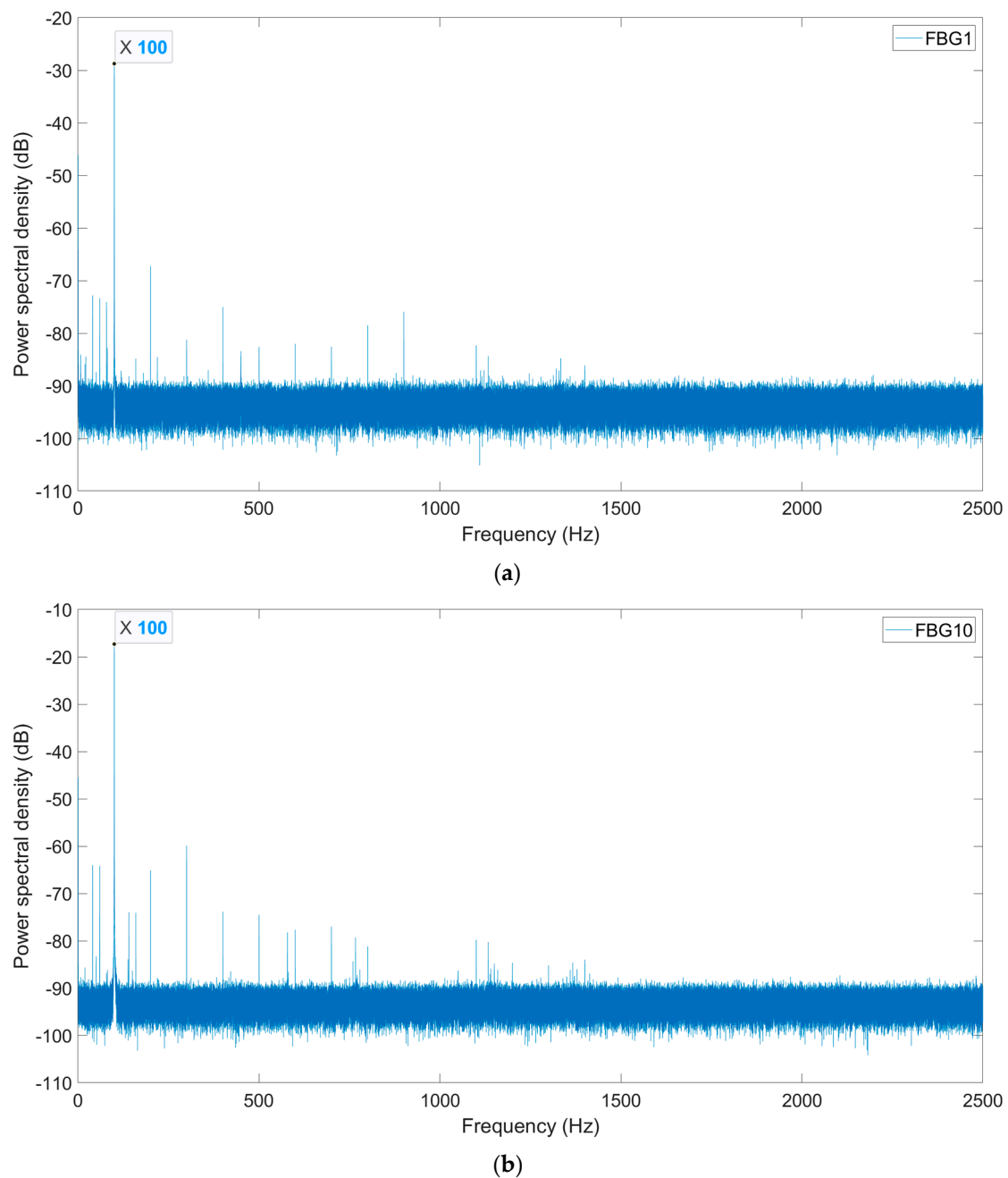


Figure 17. PSD under 100 Hz sine fixed frequency vibration condition: (a) FBG1; (b) FBG10.

It can be seen from Figure 17 that both the signal power spectra of FBG1 with slight changes and FBG10 with significant changes in the time domain can clearly identify the peak frequency of 100 Hz. This also proves the high accuracy of FBG sensors for monitoring the dynamic response of CFRP laminates.

4.2. Short-Time Fourier Transform Analysis

Although Fourier transform can identify the main frequency information of FBG signals, Fourier analysis has a very serious disadvantage. After transforming the signal from time-domain to frequency-domain, time information is lost. When using Fourier transform to analyze a specific signal, it is impossible to know which frequency corresponds to which time point it appeared at and at which time point it disappeared. This is catastrophic for the non-stationary signals monitored by FBGs, such as the FBG signals under sinusoidal

sweep, pulse sweep, and rectangular pulse conditions mentioned above. The short-time Fourier transform overcomes this drawback.

The short-time Fourier transform can be regarded as a windowed Fourier transform, and its expression is as follows [30]:

$$\text{STFT}_x(n, \omega) = \sum_{m=-\infty}^{\infty} x(m)w(n-m)e^{-j\omega m} \quad (6)$$

where $x(n)$ is the reflected signal and n is the time variable. $w(n)$ is a window function and this article uses the Hann window. Its function is to intercept a section of signal near $x(n)$ at time n , and perform Fourier transform on it. When n changes, the window function will move accordingly, thus obtaining the change rule of signal spectrum with time n . At this point, the Fourier transform becomes a (n, ω) function in a two-dimensional domain.

The time–frequency distribution diagram of the FBG signals can be obtained by short-time Fourier transform. Figure 18 shows the short-time Fourier transform diagram of FBG10 under various working conditions.

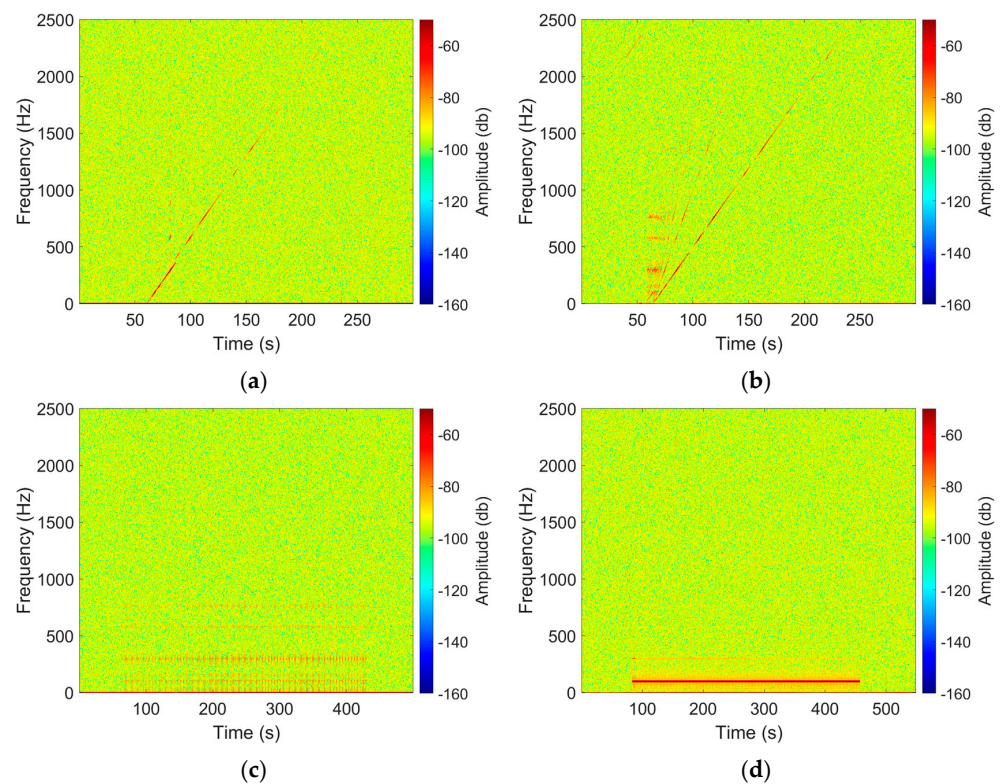


Figure 18. Short-time Fourier transform diagram of FBG signals: (a) Sine sweep condition; (b) pulse sweep condition; (c) rectangular pulse condition; (d) 100 Hz sine fixed frequency vibration condition.

From Figure 18a, we can find the time–frequency characteristics of the FBG signals under the condition of sine frequency sweep. In the time interval of 3 min from 60 s to 240 s, the frequency of the signal gradually increases from 1 Hz to 2500 Hz, which corresponds to the loading method of sine frequency sweep.

Figure 18b shows the time–frequency characteristics of the FBG signal under the condition of pulse frequency sweep. In the time interval of 3 min from 60 s to 240 s, the frequency of the signal gradually increases from 1 Hz to 2500 Hz, corresponding to the loading method of pulse frequency sweep. It is also worth noting that because the pulse sweep has a certain impact characteristic, the short-time Fourier transform diagram does not only have a straight line like the sine sweep, but also contains other frequency content,

which reflects the difference between pulse sweeping and sine sweeping on the CFRP laminates.

Figure 18c shows the time–frequency characteristics of the FBG signal under the rectangular pulse condition; the frequency blowout occurs at equal intervals in the time interval from 60 to 430 s and the frequency content is concentrated in the range of 1–800 Hz, which is consistent with the loading of the rectangular pulse corresponding to the method.

Figure 18d shows the time–frequency characteristics of FBG under the condition of 100 Hz sinusoidal fixed frequency vibration; the frequency is stable at 100 Hz in the time interval from 90 to 450 s, which corresponds to the loading mode of 100 Hz sinusoidal fixed frequency vibration.

4.3. Frequency-Domain Decomposition Analysis

In frequency-domain analysis, the identification of the modal parameters of a structure is critical for determining the state and damage of the structure. Although Fourier transform can identify the natural frequency of the structure, it is aimed at a single sensor signal, and some information will be lost for a multi-output system. Moreover, the traditional parameter identification method is based on the frequency response function under laboratory conditions. It requires simultaneous measurement of structural excitation and response signals. However, in many engineering practices, engineering conditions are quite different from laboratory conditions. It is not easy to artificially stimulate some large-scale engineering structures, and the implementation of experiments is difficult and costly. For actual large and complex structures in the working environment, traditional modal testing cannot realize online tests that do not affect the normal use of the structure, and the real-time monitoring of the inputs and the outputs of the structure is critically difficult. Therefore, it is necessary to use only output data for parameter identification of structures. The frequency domain decomposition method (FDD) used in this paper is such a method. The basic idea of FDD is to perform singular value decomposition (SVD) on the power spectral density function matrix of the structural response excited by white noise, and decompose it into the corresponding structure single-degree-of-freedom (SDOF) power spectral density function for multiple modes. The power spectral density function of the response output describes the relationship between the external stimulus input and the measured output response, which can be expressed as [31,32]:

$$\mathbf{S}_{yy}(j\omega) = \mathbf{H}(j\omega)^* \mathbf{S}_{uu}(j\omega) \mathbf{H}(j\omega)^T \quad (7)$$

where $\mathbf{S}_{uu}(j\omega)$ is the power spectral density matrix of the input signal. $\mathbf{S}_{yy}(j\omega)$ is the power spectral density matrix of the output response. $\mathbf{H}(j\omega)$ is the frequency response function. The superscript * and T represent the complex conjugate and transpose of the matrix, respectively. Under environmental excitation conditions, assuming that the input signal is a white noise signal, the singular value decomposition of $\mathbf{S}_{yy}(j\omega)$ can be obtained:

$$\mathbf{S}_{yy}(j\omega) = \mathbf{U}(j\omega) \mathbf{S}(j\omega) \mathbf{U}(j\omega)^H \quad (8)$$

where $\mathbf{U}(j\omega) = [u_1, u_2, \dots, u_m]$ is a unitary matrix containing complex vectors of singular values. The superscript H represents the calculation of the conjugate transpose of the matrix. $\mathbf{S}(j\omega)$ is a diagonal matrix containing m scalar singular values, and each singular value corresponds to the power spectrum of a single-degree-of-freedom system; m is the number of output response measuring points. The scalar diagonal matrix $\mathbf{S}(j\omega)$ sequence peaks correspond to the modal frequencies of the structure [31,32].

Since the frequency domain decomposition method requires the excitation to be close to white noise, only the sinusoidal frequency sweep, pulse frequency sweep, and rectangular pulse conditions are processed. Figure 19 shows the results of the frequency domain decomposition method.

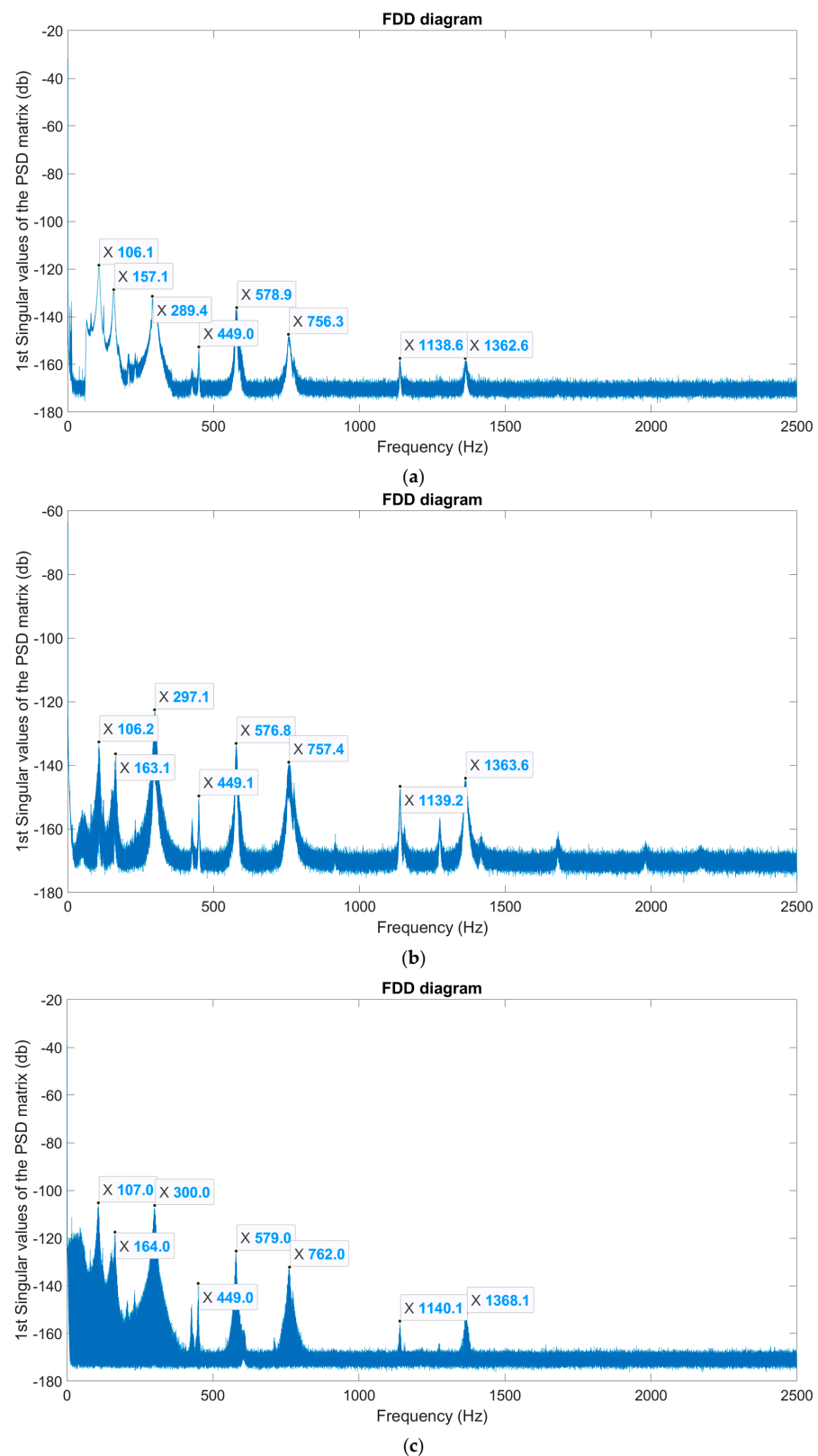


Figure 19. Frequency domain decomposition image: (a) Sine sweep condition; (b) pulse sweep condition; (c) rectangular pulse condition.

It can be found from Figure 19 that the overall trend of the modal frequency extraction diagram obtained by the frequency domain decomposition method is basically the same under different working conditions, and the peak frequencies are also similar. Table 2

shows the modal frequencies extracted under the three working conditions. It can be seen that the modal frequencies extracted under the three working conditions are basically the same, indicating that the CFRP laminates are in good condition and no obvious damage has occurred, which corresponds to the fact that the CFRP laminates had no visible damage during inspection [33]. At the same time, comparing Figures 14–16 with Figure 19, it can be seen that the frequency domain decomposition results under various working conditions have more peak frequencies than the power spectrum results of the FBG10 signal, which is more effective for the identification of natural frequencies. This is because the frequency domain decomposition method is an integrated analysis of all FBG sensor signals, while the power spectrum analysis is only for one FBG sensor.

Table 2. Comparison of modal frequency.

Working Condition	Modal Frequency (Hz)							
	106.1	157.1	289.4	449	575.9	756.3	1138.6	1362.6
Sine sweep	106.1	157.1	289.4	449	575.9	756.3	1138.6	1362.6
Pulse sweep	106.2	163.1	297.1	449.1	576.8	757.4	1139.2	1363.6
Rectangular pulse	107	164	300	449	579	762	1140.1	1368.1
Average value	106.4	161.4	295.5	449	577.2	758.6	1139.3	1364.7

5. Conclusions

To promote the development of smart optical fiber composite structures and their dynamic characteristics and damage identification methods, this paper conducted vibration experiments on CFRP laminates with FBG sensors attached to the upper and bottom surfaces under various dynamic actions. The time- and frequency-domain analyses on the FBG sensing signals during the dynamic experiment were carried out to evaluate the dynamic characteristics of the CFRP laminates and the effectiveness and reliability of the FBG sensing technology. The following conclusions can be drawn from the research:

- (1) The FBG sensors arranged on the CFRP laminates can accurately measure their dynamic response, and can judge the excited position of the CFRP laminates and invert the strain distribution of the CFRP laminates through the signal properties of FBG sensors at different positions.
- (2) The short-time Fourier transform can accurately reflect the time–frequency characteristics of the excitation of CFRP laminates under 1–2500 Hz sweep frequency, shock, and 100 Hz sinusoidal excitation from the data monitored by the FBG sensors. Both the frequency information of the excitation and the time distribution of the frequency can be simultaneously obtained.
- (3) The first eight modal frequencies of the CFRP laminates can be extracted from the FBG monitoring data by FDD, and the modal frequencies extracted under the three working conditions are basically the same. The slight difference can be attributed to noise interference. This conclusion can be further used for damage identification of CFRP laminates.
- (4) Since FBG sensors have different sensitivities for different test directions, how to ensure excellent sensing effects in an actual structure should be carefully considered. Since FBG sensors can accurately measure the strain of a CFRP structure, it is a feasible solution to reconstruct the stress–strain field of the CFRP structure through an FBG sensor array.

This paper provides valuable experimental results for the performance monitoring of CFRP structures based on FBG testing technology. In future studies, FBG sensing technology can be combined with other sensing technologies for multi-scale analysis to gain a comprehensive understanding of the performance and health status of CFRP structures. The results of this study can also be applied to practical engineering projects to verify their feasibility and effectiveness in complex environments.

Author Contributions: Methodology, H.-P.W.; Formal analysis, C.C.; Data curation, C.C. and J.M.; Writing—original draft, C.C.; Writing—review & editing, H.-P.W.; Visualization, M.W.; Supervision, H.-P.W.; Funding acquisition, H.-P.W. All authors have read and agreed to the published version of the manuscript.

Funding: The work described in this paper was supported by the National Natural Science Foundation of China (11932008 and 51908263); Provincial Projects (22YF7GA182); the Fundamental Research Funds for the Central Universities (No. lzujbky-2022-kb01); the Hunan Science Fund for Distinguished Young Scholars (2021JJ10061); and the Key R&D Program of Hunan Province (2020SK2060).

Data Availability Statement: The data supporting the results reported in the paper can be accessed from the corresponding authors.

Acknowledgments: Special thanks are due to Jinping Ou and Zhi Zhou of Dalian University of Technology, and Youhe Zhou and Ning Huang of Lanzhou University. The findings and opinions expressed in this article are only those of the authors and do not necessarily reflect the views of the sponsors.

Conflicts of Interest: The authors declare no conflict of interest.

References

1. Karataş, M.A.; Gökçaya, H. A review on machinability of carbon fiber reinforced polymer (CFRP) and glass fiber reinforced polymer (GFRP) composite materials. *Def. Technol.* **2018**, *14*, 318–326. [[CrossRef](#)]
2. Frhaan, W.K.M.; Abu Bakar, B.H.; Hilal, N.; Al-Hadithi, A.I. CFRP for strengthening and repairing reinforced concrete: A review. *Innov. Infrastruct. Solut.* **2021**, *6*, 49. [[CrossRef](#)]
3. Rajak, D.K.; Wagh, P.H.; Linul, E. Manufacturing technologies of carbon/glass fiber-reinforced polymer composites and their properties: A review. *Polymers* **2021**, *13*, 3721. [[CrossRef](#)]
4. Oehlers, D.J.; Moran, J.P. Premature failure of externally plated reinforced concrete beams. *J. Struct. Eng.* **1990**, *116*, 978–995. [[CrossRef](#)]
5. Oehlers, D.J. Reinforced concrete beams with plates glued to their soffits. *J. Struct. Eng.* **1992**, *118*, 2023–2038. [[CrossRef](#)]
6. Francesconi, L.; Taylor, M.; Bertoldi, K.; Baldi, A. Static and modal analysis of low porosity thin metallic auxetic structures using speckle interferometry and digital image correlation. *Exp. Mech.* **2018**, *58*, 283–300. [[CrossRef](#)]
7. Guinchar, M.; Angeletti, M.; Boyer, F.; Catinaccio, A.; Gargiulo, C.; Lacny, L.; Laudi, E.; Scislo, L. Experimental modal analysis of lightweight structures used in particle detectors: Optical non-contact method. In Proceedings of the 9th International Particle Accelerator Conference, IPAC18, Vancouver, BC, Canada, 29 April–4 May 2018; pp. 2565–2567.
8. Liu, H.; Zhu, Z.; Zheng, Y.; Liu, B.; Xiao, F. Experimental study on an FBG strain sensor. *Opt. Fiber Technol.* **2018**, *40*, 144–151. [[CrossRef](#)]
9. Wang, H.P.; Jiang, L.Z.; Xiang, P. Improving the durability of the optical fiber sensor based on strain transfer analysis. *Opt. Fiber Technol.* **2018**, *42*, 97–104. [[CrossRef](#)]
10. Wang, L.; Wang, Y.; Wang, J.; Li, F. A high spatial resolution FBG sensor array for measuring ocean temperature and depth. *Photonic Sens.* **2020**, *10*, 57–66. [[CrossRef](#)]
11. Wang, H.P.; Dai, J.G. Strain transfer analysis of fiber Bragg grating sensor assembled composite structures subjected to thermal loading. *Compos. Part B Eng.* **2019**, *162*, 303–313. [[CrossRef](#)]
12. Panopoulou, A.; Fransen, S.; Gomez-Molinero, V.; Kostopoulos, V. Experimental modal analysis and dynamic strain fiber Bragg gratings for structural health monitoring of composite antenna sub-reflector. *CEAS Space J.* **2013**, *5*, 57–73. [[CrossRef](#)]
13. Tserpes, K.I.; Karachalios, V.; Giannopoulos, I.; Prentzias, V.; Ruzek, R. Strain and damage monitoring in CFRP fuselage panels using fiber Bragg grating sensors. Part I: Design, manufacturing and impact testing. *Compos. Struct.* **2014**, *107*, 726–736. [[CrossRef](#)]
14. Ruzek, R.; Kudrna, P.; Kadlec, M.; Karachalios, V.; Tserpes, K.I. Strain and damage monitoring in CFRP fuselage panels using fiber Bragg grating sensors. Part II: Mechanical testing and validation. *Compos. Struct.* **2014**, *107*, 737–744. [[CrossRef](#)]
15. Lu, S.; Jiang, M.; Sui, Q.; Sai, Y.; Jia, L. Damage identification system of CFRP using fiber Bragg grating sensors. *Compos. Struct.* **2015**, *125*, 400–406. [[CrossRef](#)]
16. Lu, S.; Jiang, M.; Sui, Q.; Sai, Y.; Jia, L. Low velocity impact localization system of CFRP using fiber Bragg grating sensors. *Opt. Fiber Technol.* **2015**, *21*, 13–19. [[CrossRef](#)]
17. Rezayat, A.; De Pauw, B.; Lamberti, A.; El-Kafafy, M.; Nassiri, V.; Ertveldt, J.; Arroud, G.; Vanlanduit, S.; Guillaume, P. Reconstruction of impacts on a composite plate using fiber Bragg gratings (FBG) and inverse methods. *Compos. Struct.* **2016**, *149*, 1–10. [[CrossRef](#)]
18. Zhao, G.; Li, S.; Hu, H.; Zhong, Y.; Li, K. Impact localization on composite laminates using fiber Bragg grating sensors and a novel technique based on strain amplitude. *Opt. Fiber Technol.* **2018**, *40*, 172–179. [[CrossRef](#)]
19. Geng, X.; Lu, S.; Jiang, M.; Sui, Q.; Lv, S.; Xiao, H.; Jia, Y.; Jia, L. Research on FBG-based CFRP structural damage identification using BP neural network. *Photonic Sens.* **2018**, *8*, 168–175. [[CrossRef](#)]

20. Datta, A.; Augustin, M.J.; Gupta, N.; Viswamurthy, S.R.; Gaddikeri, K.M.; Sundaram, R. Impact localization and severity estimation on composite structure using fiber Bragg grating sensors by least square support vector regression. *IEEE Sens. J.* **2019**, *19*, 4463–4470. [[CrossRef](#)]
21. Falcetelli, F.; Martini, A.; Di Sante, R.; Troncosi, M. Strain modal testing with fiber bragg gratings for automotive applications. *Sensors* **2022**, *22*, 946. [[CrossRef](#)] [[PubMed](#)]
22. Wang, H.P.; Ni, Y.Q.; Dai, J.G.; Yuan, M.D. Interfacial debonding detection of strengthened steel structures by using smart CFRP-FBG composites. *Smart Mater. Struct.* **2019**, *28*, 115001. [[CrossRef](#)]
23. Geng, X.; Jiang, M.; Gao, L.; Wang, Q.; Jia, Y.; Sui, Q.; Jia, L.; Li, D. Sensing characteristics of FBG sensor embedded in CFRP laminate. *Measurement* **2017**, *98*, 199–204. [[CrossRef](#)]
24. Liu, Y.; Liu, X.; Zhang, T.; Zhang, W. Integrated FPI-FBG composite all-fiber sensor for simultaneous measurement of liquid refractive index and temperature. *Opt. Lasers Eng.* **2018**, *111*, 167–171. [[CrossRef](#)]
25. Wang, H.; Xiang, P.; Li, X. Theoretical analysis on strain transfer error of FBG sensors attached on steel structures subjected to fatigue load. *Strain* **2016**, *52*, 522–530. [[CrossRef](#)]
26. Wang, H.; Jiang, L.; Xiang, P. Priority design parameters of industrialized optical fiber sensors in civil engineering. *Opt. Laser Technol.* **2018**, *100*, 119–128. [[CrossRef](#)]
27. Meng, Q.; Sen, D.; Wang, S.; Hayes, L. Impulse response measurement with sine sweeps and amplitude modulation schemes. In Proceedings of the 2008 2nd International Conference on Signal Processing and Communication Systems, Gold Coast, Australia, 15–17 December 2008; pp. 1–5.
28. Weiss, G.H.; Gitterman, M. Motion in a periodic potential driven by rectangular pulses. *J. Stat. Phys.* **1993**, *70*, 93–105. [[CrossRef](#)]
29. Youngworth, R.N.; Gallagher, B.B.; Stamper, B.L. An overview of power spectral density (PSD) calculations. In *Optical Manufacturing and Testing VI, Proceedings of the SPIE 2005, San Diego, CA, USA, 31 July–4 August 2005*; SPIE: Bellingham, WA, USA, 2005; Volume 5869, pp. 206–216.
30. Nawab, S.; Quatieri, T.; Lim, J. Signal reconstruction from short-time Fourier transform magnitude. *IEEE Trans. Acoust. Speech Signal Process.* **1983**, *31*, 986–998. [[CrossRef](#)]
31. Brincker, R.; Zhang, L.; Andersen, P. Modal identification of output-only systems using frequency domain decomposition. *Smart Mater. Struct.* **2001**, *10*, 441. [[CrossRef](#)]
32. Amador, S.D.R.; Brincker, R. Robust multi-dataset identification with frequency domain decomposition. *J. Sound Vib.* **2021**, *508*, 116207. [[CrossRef](#)]
33. Wang, H.-P.; Chen, C.; Ni, Y.-Q.; Jayawickrema, M.; Epaarachchi, J. Computer-aided feature recognition of CFRP plates based on real-time strain fields reflected from FBG measured signals. *Compos. Part B Eng.* **2023**, *263*, 110866. [[CrossRef](#)]

Disclaimer/Publisher’s Note: The statements, opinions and data contained in all publications are solely those of the individual author(s) and contributor(s) and not of MDPI and/or the editor(s). MDPI and/or the editor(s) disclaim responsibility for any injury to people or property resulting from any ideas, methods, instructions or products referred to in the content.